Journal of ELECTRONIC MATERIALS, Vol. 46, No. 7, 2017
DOI: 10.1007/s11664-017-5428-6

Effect of Postannealing Treatment on Structural and Optical Properties of ZnO Nanorods Prepared Using Chemical Bath Deposition

SHAKER A. BIDIER,[1,2,3] M.R. HASHIM,[1,2] and AHMAD M. ALDIABAT[1,2]

1.—Institute of Nano-optoelectronics Research & Technology Laboratory (INOR), sains@usm, 11900 Penang, Malaysia. 2.—School of Physics, Universiti Sains Malaysia (USM), 11800 Penang, Malaysia. 3.—e-mail: shbidier@gmail.com

ZnO nanorods have been synthesized on glass substrate by the chemical bath deposition technique. To investigate the effect of postannealing treatment on their crystalline and optical quality, the films were annealed at various temperatures of 300°C, 400°C, and 500°C in air ambient for 1 h. The morphological and chemical composition of the ZnO films were investigated using field-emission scanning electron microscopy (FESEM) with energy-dispersive spectroscopy (EDS). The structural properties were characterized by employing x-ray diffraction analysis and Raman spectroscopy. Finally, the optical properties were investigated by photoluminescence measurements. FESEM images revealed high-quality ZnO nanorods grown on the substrate surface. EDS results demonstrated a slight reduction in the quantity of oxygen after annealing. XRD and Raman results showed noticeable improvement in the crystalline quality of the ZnO films after annealing. The crystallite size increased significantly after annealing, from 40.5 nm for the nonannealed film to a maximum for 46.2 nm for the annealed samples. The photoluminescence results exhibited an increment in the optical quality [ultraviolet (UV) versus visible emission] after postannealing treatment. The enhancement in the crystalline and optical quality of the annealed films compared with the nonannealed sample is due to recrystallization of ZnO particles into a ZnO wurtzite lattice structure as well as relaxation of oxygen molecules adsorbed on the surface of the ZnO nanorods. This enhancement is conducive to improved efficiency for potential applications of ZnO.

Key words: ZnO, nanorods, postannealing treatment, structural properties, optical quality

INTRODUCTION

Zinc oxide (ZnO) is an *n*-type II–VI semiconductor with direct wide bandgap (3.37 eV) and large binding energy (60 eV) at room temperature.[1] Recently, ZnO has attracted extensive interest from researchers due to its advantages such as low cost,[2] nontoxicity, as well as chemical and thermal stability.[3] ZnO is a promising material for use in several potential applications in various fields such as light-emitting diodes, photodetectors, solar cells, and gas sensors.[4,5]

ZnO nanostructures have previously been synthesized using numerous techniques such as chemical vapor deposition (CVD),[6] radiofrequency (RF) magnetron sputtering,[7] and metalorganic chemical vapor deposition (MO-CVD).[8] In contrast to these methods, chemical bath deposition (CBD) offers several advantages such as simple and low-cost setup, low-temperature deposition, suitability for large-scale production, and facile control of deposition conditions.[9,10] ZnO nanostructures prepared through low-temperature CBD, however, show

(Received October 5, 2016; accepted March 1, 2017; published online March 17, 2017)

various structural and surface defects which reduce the film quality and its performance in potential applications.[11]

The structural properties of ZnO are affected by intrinsic defects such as vacancies and interstitials. Presence of vacancies or interstitials in as-prepared film may reduce/expand the lattice parameters in comparison with unstrained film. This may generate compressive/tensile strain, in turn reducing the crystalline quality. These defects (including oxygen vacancies, oxygen, and Zn interstitials) may enhance the visible emission that is ascribed to recombination of photogenerated electrons.[12–14] In addition, surface defects, such as adsorbed molecules (M_{ad}) on the surface of the nanorods, could be generated, for example, oxygen or OH group. These defects may reduce optical luminescence via a nonradiative process between electrons with M_{ad} at the surface. This nonradiative process reduces the optical quality because photogenerated electrons are captured by M_{ad} instead of recombining with holes in the valence band.[15,16]

Postannealing treatment (PAT) is a promising process suggested to reduce the defects generated in deposited films. Various studies have reported that postannealing treatment can be employed to improve the structural and optical properties of ZnO nanostructures. Recently, the effect of postannealing treatment on the photoluminescence of ZnO nanorods prepared by the hydrothermal method was studied. As-grown ZnO nanorods were annealed in nitrogen and oxygen at 800°C. The results showed strong enhancement of ultraviolet (UV) emission as well as improvement in the crystalline quality after annealing treatment.[11] In addition, the effect of the postannealing process on the structural and optical properties of ZnO thin films prepared by the sol-gel method has been investigated. As-grown films were annealed at various temperatures from 300°C to 1000°C in oxygen ambient. The findings demonstrated that annealing at temperature of 550°C to 700°C improved the film quality; however, annealing at higher temperature of 700°C to 1000°C reduced the film quality.[17]

In the present work, the effect of PAT on the structural and optical properties of ZnO nanorods (NRs) prepared by the CBD method was investigated. The objectives of this work include use of simple procedures and the low-cost CBD method to synthesize ZnO NRs, study of the effects of PAT on their structural and optical properties related to intrinsic and surface defects, and finally determination of the optimum temperature for PAT in air ambient to improve their structural and optical properties; this will lead to further research and enable potential applications of ZnO NRs formed by simple and cost-effective methods.

PREPARATION OF ZNO FILMS

A medical glass substrate was cut into 2 cm × 1 cm pieces, followed by surface cleaning using an ultrasonic pot with acetone for 10 min. The substrate was then rinsed with deionized (DI) water and dried using nitrogen gas. Afterwards, the substrates were seeded with a 50-nm layer of ZnO using a ZnO target (99.999% purity) in a radiofrequency sputtering system (HHV-Auto500) at room temperature in Ar gas ambient. The working power and pressure were 150 W and 7.47×10^{-4} kPa, respectively.

Zn nitrate hexahydrate [$Zn(NO_3)_2{\cdot}6H_2O$, 20 mM; Sigma-Aldrich] with equimolar concentration of hexamethylenetetramine (HMTM, $C_6H_{12}N_4$; Sigma-Aldrich) were dissolved in 80 ml DI water in a beaker. The seeded substrates were suspended vertically in the beaker containing the solution. The beaker was subsequently placed in a furnace oven at 93°C for 5 h. Finally, the substrates were removed and washed with DI water for 5 min, then dried using nitrogen gas. The day after, the as-grown samples were annealed at different temperatures of 300°C, 400°C, and 500°C for 1 h in air ambient. As-deposited and annealed samples were then subjected to further characterization.

CHARACTERIZATION

The morphological features of the as-deposited films were investigated using field-emission scanning electron microscopy (FESEM; FEI Nova NanoSEM 450) with energy-dispersive spectroscopy (EDS). Structural characterization was performed by high-resolution x-ray diffraction (HR-XRD) analysis using a PANalytical X'PertPRO MRD system equipped with a Cu K_α radiation source (λ = 0.15406 nm), operated at 40 kV and 20 mA. Photoluminescence (PL) measurements were conducted by employing a He–Cd laser (325 nm) at room temperature. Raman spectra were recorded by utilizing a HORIBA Jobin Yvon HR800 Raman spectrometer with Ar^+ ion laser as excitation source operating at wavelength of 514.55 nm and power of 20 mW.

RESULTS AND DISCUSSION

Morphological Observations

Figure 1 shows top-view FESEM images of the as-grown ZnO thin film and ZnO thin films after PAT at temperature of 300°C, 400°C, and 500°C for 1 h in air atmosphere. These typical FESEM images reveal that all the ZnO thin films were uniform with compact nanorod arrays grown vertically on the glass substrate. The nanorods were grown on large scale, indicating that synthesis of ZnO nanorods using the CBD method is suitable for industrial application, indicating good deposition conditions, e.g., uniform heat distribution, and suitable precursor concentrations. No noteworthy changes in morphological characteristics were observed in the annealed films compared with the as-deposited sample. This could be due to the moderate

annealing temperature used in this work (up to 500°C, as compared with the high melting point of ZnO of 1975°C[18]), preventing changes in the morphology of the ZnO nanorods. Previously, ZnO nanorods were annealed at high temperature of 450°C,[19] 700°C,[20] or 800°C,[21] with no changes in morphological features being observed.

In the CBD method, the ZnO nanostructures are synthesized via Reactions 1–5.[4] The first and second equations describe the reaction of HMTM with H_2O to form a basic solution through generation of OH^- ions. Next, OH^- ions react with Zn^{2+} ions to produce $Zn(OH)_2$. Finally, $Zn(OH)_2$ is dehydrated to produce ZnO, as shown in Eq. 5. The thermal energy provided from the deposition pot plays an important role in releasing HMTM to generate OH^- ions, as well as the decomposition of $Zn(OH)_2$ to form ZnO. The final ZnO molecule represents the basic unit to form the lattice structure.[3,22]

$$C_6H_{12}N_4 + 6H_2O \rightarrow 6HCHO + 4NH_3 \quad (1)$$

$$NH_3 + H_2O \rightarrow NH_4^+ + OH^- \quad (2)$$

$$Zn(NO_3)_2 \rightarrow Zn^{+2} + 2NO_3^- \quad (3)$$

$$Zn^{+2} + 2OH^- \rightarrow Zn(OH)_2 \quad (4)$$

$$Zn(OH)_2 \xrightarrow{\Delta} ZnO + H_2O \quad (5)$$

The chemical composition of the ZnO films was characterized by EDS (Fig. 2a). The quantity of oxygen was reduced after annealing (Fig. 2b), indicating that oxygen molecules adsorbed at the surface of the nanorods were released. The thermal energy generated in the annealing process could have repelled these molecules from the surface of the nanorods.

XRD ANALYSIS

Figure 3 shows typical XRD patterns for the ZnO nanorods synthesized on glass substrate using the CBD method at 93°C for 5 h with postannealing at different temperatures in air ambient for 1 h. All samples exhibited one major (002) peak, indicating

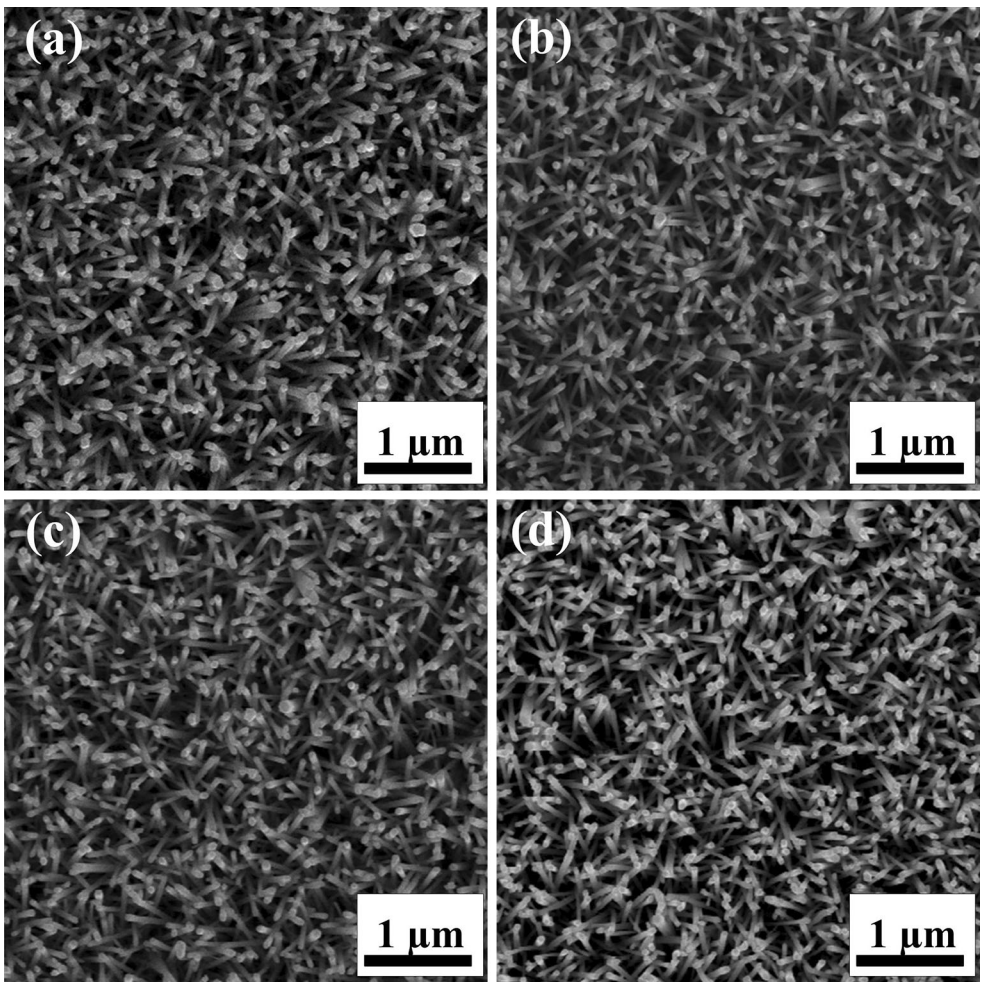

Fig. 1. FESEM images of ZnO nanorods: (a) nonannealed film, (b) annealed at 300°C, (c) annealed at 400°C, and (d) annealed at 500°C.

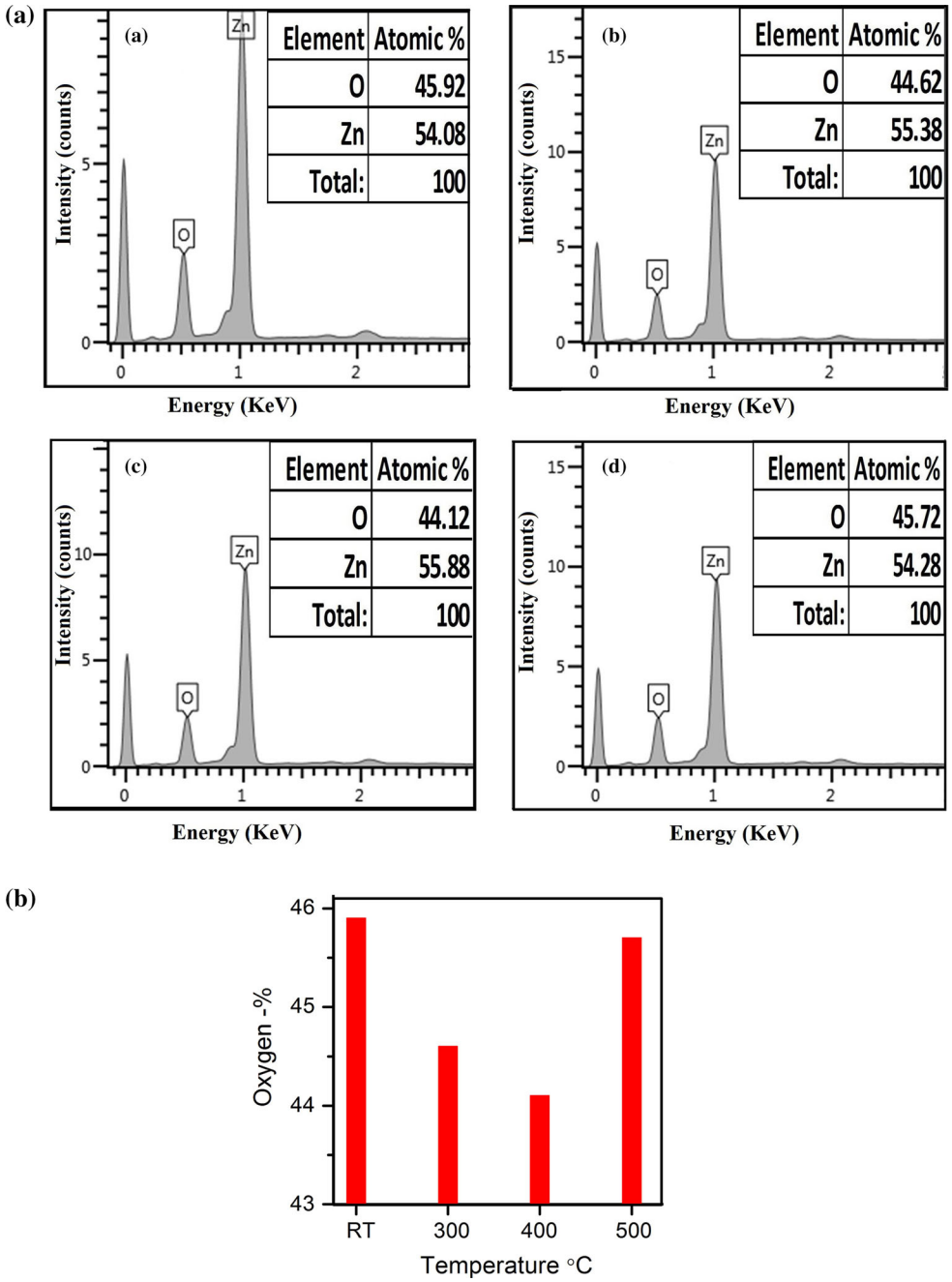

Fig. 2. **a** EDS spectra of ZnO nanorods: (a) nonannealed film, (b) annealed at 300°C, (c) annealed at 400°C, and (d) annealed at 500°C. **b** Oxygen atomic percentages in non- and postannealed ZnO films.

high crystalline quality with wurtzite hexagonal structure phase, matching Joint Committee on Powder Diffraction Standards (JCPDS) card no. 01-080-0074. It was noted that the *c*-axis was the preferred growth direction. No impurity peaks or peaks from other phases are seen in these results, indicating that the samples had good purity.

The intensity of (002) peak increased as the annealed temperature was increased. PAT provides atoms with thermal energy, promoting their occupation at the correct locations in the lattice crystal. Because the (002) orientation has the lowest surface free energy, the atoms tended to coordinate into this direction, resulting in enhanced ZnO crystalline quality.[17]

The inset in Fig. 3 shows a slight shift towards smaller angle of the (002) peak for the annealed samples, as compared with pure ZnO. The crystallite size D of the as-grown samples was calculated from (002) peak using Scherrer's formula in[23] Eq. 6. Equation 7 was employed for the lattice constant c, and Eq. 8 was used to calculate the strain (ε_{zz}).

$$D = 0.9\lambda/\beta\cos\theta, \quad (6)$$

$$c = \lambda/\sin\theta, \quad (7)$$

$$\varepsilon_{zz} = \frac{c - c_0}{c_0} \times 100\%. \quad (8)$$

D represents the crystallite size, λ is the wavelength of the x-ray source (0.15406 Å), β is the full-width at half-maximum (FWHM) of (002) peak, θ is the diffraction angle of (002) peak, c is the lattice constant, and c_0 is the unstrained lattice constant (0.52125 nm). The lattice parameters are presented in Table I.

The FWHM value reflects the crystallinity of the as-prepared film. Note that the FWHM reduced sharply for the annealed samples compared with the nonannealed film, indicating improved crystallinity of the films after annealing treatment. Similar findings were reported previously.[24,25]

The crystallite size increased after annealing, from 40.5 nm for the nonannealed ZnO to 45.2 nm, 46.2 nm, and 45.5 nm for films annealed at temperature of 300°C, 400°C, and 500°C, respectively. This may be due to recrystallization of the atoms of ZnO into ZnO wurtzite lattice structure due to thermal energy generated by PAT. This energy helps atoms to arrange themselves into the plane with lowest free surface energy, i.e., (002),[26] or the small crystallites coalesced after annealing to form larger crystallites.[27] The crystallite size decreased for annealing temperature of 500°C. This may be due to splitting of Zn–O bond.[17]

A slight increase in the lattice constant was found after the annealing process, from 0.51974 nm for the nonannealed sample to 0.52028 nm, 0.5227 nm, and 0.52024 nm for the samples annealed at temperature of 300°C, 400°C, and 500°C, respectively. This increment in the lattice constant indicates relaxation of internal strain due to thermal energy generated by the annealing process.[28] The nonannealed sample demonstrated a negative strain value, indicating compressive strain. The postannealed samples also showed compressive strain, with values lower than that for the nonannealed sample. During the postannealing process, thermal energy assists lattice atoms to correct their locations, leading to the increase in the lattice constant and the decrease in compressive strain.[25,26]

RAMAN ANALYSIS

Raman spectroscopy is a powerful technique for studying the crystalline structure of materials, providing useful information on the crystalline properties, defects, and strain of as-grown films. Figure 4 shows the Raman spectra measured using the 514.55-nm laser source at power of 20 mW. It can be seen that there are two characteristic peaks.

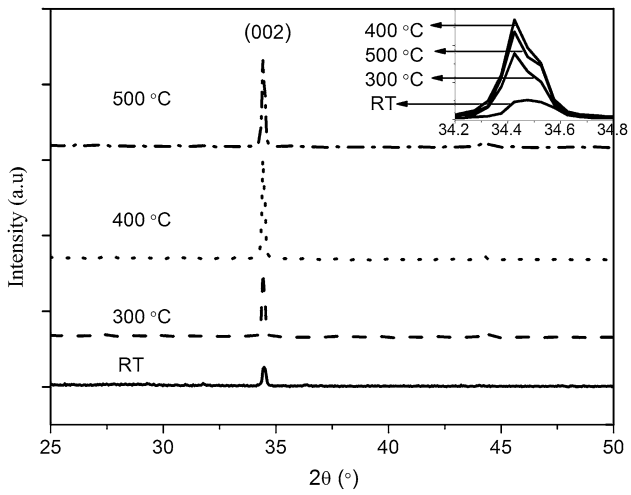

Fig. 3. XRD patterns of non- and postannealed ZnO films.

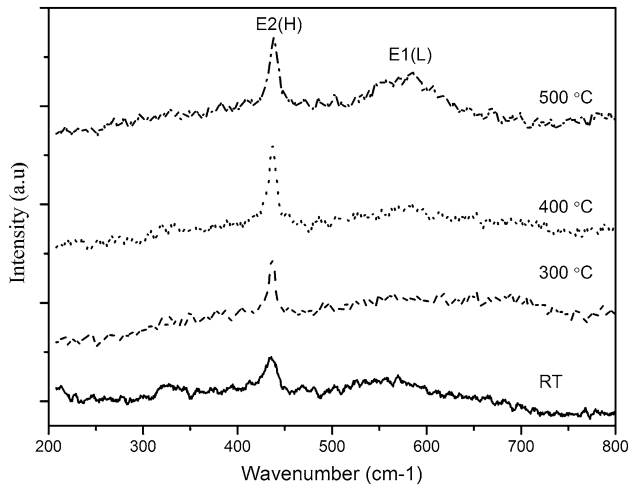

Fig. 4. Raman shifts of non- and postannealed ZnO films.

Table I. (002) peak position, FWHM, crystallite size, and lattice parameter c calculated from XRD analysis

Annealing Temperature (°C)	2θ (°)	FWHM (°)	D (nm)	c (nm)	ε_{zz} (%)
0	34.485	0.187	40.5	0.51974	−0.219
300	34.448	0.1680	45.2	0.52028	−0.186
400	34.449	0.1643	46.2	0.52027	−0.188
500	34.451	0.1668	45.5	0.52024	−0.193

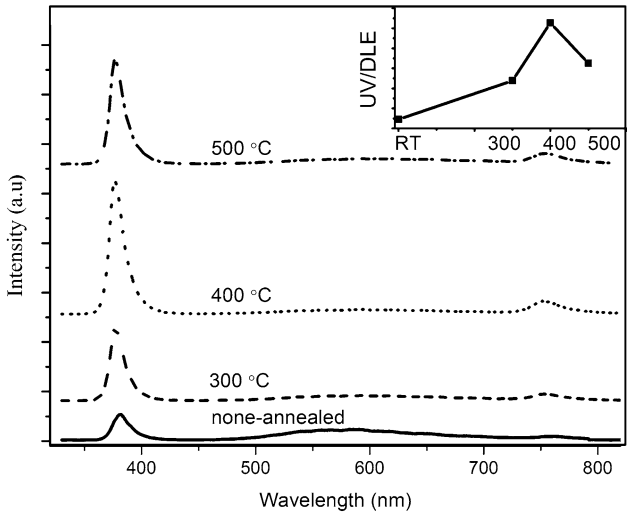

Fig. 5. Room-temperature PL spectra of non- and postannealed ZnO films.

One of these, i.e., E2(H), corresponds to hexagonal wurtzite-type structure, while the other, called E1(L), can be attributed to defects in the lattice structure.[4] After PAT at 300°C, the intensity of the E2(H) peak increased while the intensity of E1(L) decreased, indicating improved crystalline quality due to decreased defects. For the sample annealed at 400°C, the E2(H) signal increased significantly with quenching of E1(L). However, at the higher annealing temperature of 500°C, the intensity of E2(H) began to decrease while the intensity of E1(L) strongly increased, indicating degradation in the crystalline quality with increased defects when the sample was annealed at high temperature of 500°C. The increment in the E2(H) peak intensity and the reduction of the intensity of E1(L) for the samples annealed at 300°C and 400°C is attributed to restructuring of ZnO atoms to their correct sites in the ZnO lattice, as mentioned in "XRD Analysis" section. However, the reduction in the E2(H) intensity with increasing E1(L) intensity indicates bond breakage in ZnO due to high annealing temperature, which increased defects such as interstitials and vacancies. Recently, ZnO nanostructures were postannealed at various temperatures of 400°C[27] as well as 300°C, 600°C, and 900°C;[29] both of those studies reported strong enhancement of E2(H) peak, indicated improved crystalline quality. Simultaneously, the defect-related peak, i.e., E1(L), also increased, indicating an increase in defects after the annealing process. However, in this work, E2(H) increased while E1(L) decreased for the samples annealed at 300°C and 400°C, demonstrating that good annealing conditions were used in this study.

PL ANALYSIS

Figure 5 shows the PL spectra of the as-prepared and postannealed ZnO films recorded at room temperature. All films showed two peaks. The strong peak located in the UV region corresponds to radiative recombination of electrons with holes in the valence band. Its intensity significantly increased as the annealing temperature was increased. Another peak located in the visible region corresponds to photogenerated electrons trapped by deep defects within the bandgap, such as vacancies (V_{Zn}, V_O) and interstitials (Zn_i, O_i), also known as deep-level emission (DLE).[30] It can be seen that the DLE was quenched after annealing, resulting from a reduction in the previous defects after annealing treatment; similar results were reported previously.[28]

The optical quality (UV/DLE) was calculated from the PL results and is visualized in the inset of Fig. 5. As the annealing temperature was increased, the optical quality strongly increased as well. The nonannealed sample had optical quality of 2.27, while the films annealed at temperature of 300°C, 400°C, and 500°C had optical quality of 11.93, 26.35, and 16.27, respectively. All the annealed samples showed better optical quality compared with the nonannealed film, indicating improved optical properties after annealing treatment was conducted. This enhancement in optical quality corresponds to the improvement in the crystalline quality.[25] The sample annealed at 400°C demonstrated the highest optical quality, but the sample annealed at 500°C showed a sharp reduction in optical quality compared with that annealed at 400°C. This decrease in optical quality at high annealing temperature results from the degradation in crystalline quality as mentioned in "XRD Analysis" section.

When a ZnO sample is exposed to the PL laser, electrons in the valence band are excited to the conduction band. After the laser is switched off, excited electrons recombine with holes in the valence band (generating UV emission) and/or with point defects in the bandgap [generating defect-related emission (DLE)]. Finally, they may be trapped by M_{ad} at the surface of the nanorods via a nonradiative process. The presence of M_{ad} at the surface of the nanorods plays a crucial role in both radiative and nonradiative processes in the ZnO nanostructures.[27,31] Since the UV emission is generated via recombination of electrons with holes in the valence band, the nonradiative recombination (electron–M_{ad}) at the surface reduces the number of electrons which can recombine with holes in the valence band, reducing the UV emission intensity. This behavior usually occurs in nonannealed samples.[11,15,32]

Annealing expels M_{ad} from the surface of the nanorods by providing thermal energy that can break electron–M_{ad} bonds, enabling trapped electrons to return to the conduction band. This process increases the number of electrons that can recombine with holes in the valence band, enhancing the intensity of the UV emission accordingly. The UV intensity decreased while the defect emission

increased at the high annealing temperature of 500°C. This may be due to the degradation of the structural quality with increase of the annealing temperature, which may break Zn–O bonds and thus increase the defects, as mentioned in "XRD Analysis" section.

Electrons generated by the annealing treatment occupy the lowest energy states in the conduction band, resulting in an increase in the energy difference between the top of the valence band and the lowest empty levels of the conduction band. This may have increased the energy bandgap after the annealing treatment, as shown in Fig. 4. This phenomenon is called the Burstein–Moss (BM) effect.[33]

EDS was used to measure the quantity of oxygen in the ZnO, consisting of oxygen atoms localized in the wurtzite lattice structure ($O_{lattice}$), interstitial oxygen atoms (O_i), and oxygen in adsorbed molecules such as O_2 and OH. However, the EDS results showed no hydrogen, so it is likely that the adsorbed molecule was O_2.

The EDS results portrayed a decrease in the quantity of O. Additionally, the XRD and PL results indicated a reduction in oxygen vacancies, indicating that thermal energy was required to help O_i settle into oxygen vacancies via a recrystallization process. As a result, there was an increase in $O_{lattice}$ and a decrease in O_i. However, this did not change the overall quantity of oxygen. In conclusion, the reduction in the quantity of oxygen resulted from removal of adsorbed oxygen molecules from the surface of the nanorods due to the thermal energy provided, resulting in reduced surface defects and thereby improved film quality. Annealing at high temperature of 500°C resulted in an increase in oxygen compared with the sample annealed at 400°C, resulting from breakage of Zn–O bonds, which increased the quantity of O_i. Creation of O_i also produces oxygen vacancies, which degraded the crystalline and optical quality, as shown by the XRD, Raman, and PL analyses.

CONCLUSIONS

We investigated the effect of postannealing on the structural and optical properties of ZnO nanorods synthesized chemically on glass substrate. The deposited films were annealed at temperature of 300°C, 400°C or 500°C in air ambient for 1 h. XRD and Raman results showed a noticeable improvement in the crystalline properties of the ZnO film after annealing. Photoluminescence results showed a strong increment in the optical quality (UV/visible emission) after postannealing treatment. The enhancement in the crystalline and optical quality of the annealed films compared with the nonannealed sample results from recrystallization of ZnO molecules into the ZnO wurtzite lattice structure as well as relaxation of adsorbed oxygen molecules at the surface of the ZnO nanorods. Such enhancement is crucial for those working to improve the efficiency of ZnO-related applications.

ACKNOWLEDGEMENT

The authors gratefully acknowledge the financial support provided by the Institute of Postgraduate Studies (IPS) Universiti Sains Malaysia (USM) Fellowship and Institute of Nano-optoelectronics Research & Technology Laboratory (INOR), sains@usm, under Grant No. 1001/CINOR/811239.

REFERENCES

1. N. Hassan, M. Hashim, and Y. Al-Douri, *Opt.-Int. J. Light Electron Opt.* 125, 2560 (2014).
2. F. Jiménez-García, C. Londoño-Calderón, D. Espinosa-Arbeláez, A. Del Real, and M. Rodríguez-García, *Bull. Mater. Sci.* 37, 1283 (2014).
3. S. Xu and Z.L. Wang, *Nano Res.* 4, 1013 (2011).
4. J. Hassan, Z. Hassan, and H. Abu-Hassan, *J. Alloys Compd.* 509, 6711 (2011).
5. L. Vayssieres, *Adv. Mater.* 15, 464–466 (2003).
6. H. Deng, J. Russell, R. Lamb, B. Jiang, Y. Li, and X. Zhou, *Thin Solid Films* 458, 43 (2004).
7. A. Samavati, H. Nur, A.F. Ismail, and Z. Othaman, *J. Alloys Compd.* 671, 170 (2016).
8. M. Boukadhaba, A. Fouzri, V. Sallet, S. Hassani, G. Amiri, A. Lusson, and M. Oumezzine, *Superlattices Microstruct.* 85, 820 (2015).
9. Y. Kumar, A.K. Rana, P. Bhojane, M. Pusty, V. Bagwe, S. Sen, and P.M. Shirage, *Mater. Res. Express* 2, 105017 (2015).
10. S.A. Bidier, M. Hashim, A.M. AL-Diabat, and M. Bououdina, *Phys. E: Low-Dimens. Sys. Nanostruct* 88, 169 (2017).
11. S.J. Chua, K.P. Loh, and E. Fitzgerald, *J. Cryst. Growth* 287, 157 (2006).
12. K. Vanheusden, C. Seager, W.T. Warren, D. Tallant, and J. Voigt, *Appl. Phys. Lett.* 68, 403 (1996).
13. B. Lin, Z. Fu, and Y. Jia, *Appl. Phys. Lett.* 79, 943 (2001).
14. M. Gomi, N. Oohira, K. Ozaki, and M. Koyano, *Jpn. J. Appl. Phys.* 42, 481 (2003).
15. A. van Dijken, E.A. Meulenkamp, D. Vanmaekelbergh, and A. Meijerink, *J. Phys. Chem. B* 104, 1715 (2000).
16. A. Stoneham, *Rep. Prog. Phys.* 44, 1251 (1981).
17. A. Singh, D. Kumar, P. Khanna, M. Kumar, and B. Prasad, *J. Mater. Sci. Mater. Electron.* 24, 4607 (2013).
18. M. Asadian, *J. Cryst. Process. Technol.* 3, 75 (2013).
19. A. Kyaw, H. Sun, X. Sun, Z. Huang and X. Zeng, *presented at the Photo. Global Conf. (PGC)*, 2010.
20. L.-L. Yang, Q. Zhao, M. Willander, J. Yang, and I. Ivanov, *J. Appl. Phys.* 105, 053503 (2009).
21. C.-W. Liu, S.-J. Chang, C.-H. Hsiao, R.-J. Huang, Y.-S. Lin, M.-C. Su, P.-H. Wang, and K.-Y. Lo, *IEEE Photonics Technol. Lett.* 26, 789 (2014).
22. L. Zhang, Y. Ruan, Y. Liu, and Y. Zhai, *Cryst. Res. Technol.* 48, 996 (2013).
23. O.F. Farhat, M.M. Halim, M.J. Abdullah, M.K. Ali, and N.K. Allam, *Beilstein J. Nanotechnol.* 6, 720 (2015).
24. R. Shabannia, *J. Mater. Sci. Mater. Electron.* 27, 6413 (2016).
25. S. Xue, H. Zhuang, C. Xue, L. Hu, B. Li, and S. Zhang, *J. Electron. Mater.* 36, 502 (2007).
26. H.S. Kang, J.S. Kang, S.S. Pang, E.S. Shim, and S.Y. Lee, *Mater. Sci. Eng. B* 102, 313 (2003).
27. D.-R. Hang, S.E. Islam, K.H. Sharma, S.-W. Kuo, C.-Z. Zhang, and J.-J. Wang, *Nanoscale Res. Lett.* 9, 1 (2014).
28. G.N. Narayanan, R.S. Ganesh, and A. Karthigeyan, *Thin Solid Films* 598, 39 (2016).
29. G.H. Mhlongo, D.E. Motaung, S.S. Nkosi, H. Swart, G.F. Malgas, K.T. Hillie, and B.W. Mwakikunga, *Appl. Surf. Sci.* 293, 62 (2014).

30. B. Panigrahy, M. Aslam, D.S. Misra, M. Ghosh, and D. Bahadur, *Adv. Funct. Mater.* 20, 1161 (2010).
31. W.-K. Hong, J.I. Sohn, S.N. Cha, J.M. Kim, and M.E. Welland, *Appl. Surf. Sci.* 324, 512 (2015).
32. S. Chen, J. Chen, J. Liu, J. Qi, and Y. Wang, *Appl. Surf. Sci.* 357, 413 (2015).
33. B.E. Sernelius, K.-F. Berggren, Z.-C. Jin, I. Hamberg, and C. Granqvist, *Phys. Rev. B* 37, 10244 (1988).